

Electronic Supplementary Information (ESI) for Chemical Communications

This journal is (c) The Royal Society of Chemistry 2018

Covalent functionalization of reduced graphene oxide aerogels with polyaniline for high performance supercapacitors

Ruijun Li, Yue Yang, Datong Wu, Kelin Li, Yong Qin, Yongxin Tao and Yong Kong*

Jiangsu Key Laboratory of Advanced Materials and Technology, School of Petrochemical Engineering, Changzhou University, Changzhou 213164, China

Email: yzkongyong@126.com

Tel.: 86-519-86330253; fax: 86-519-86330167.

Experimental section

Reagents and apparatus. Natural graphite flakes (99.95%, 325 mesh) were received from Qingdao Graphite Co., Ltd. (Qingdao, China). p-Aminobenzonic acid, ammonium persulfate (APS), aniline and ethylene glycol were purchased from Aladdin Chemistry Co., Ltd. (Shanghai, China). Ammonia water, sodium nitrite (NaNO_2), potassium permanganate (KMnO_4), concentrated sulfuric acid, phosphoric acid, methyl alcohol and concentrated hydrochloric acid were obtained from Sinopharm Chemical Reagent Co., Ltd. (Shanghai, China). All solutions were prepared with ultrapure water (Milli-Q, Millipore).

FT-IR spectra of different samples were recorded on a FTIR-8400S spectrometer (Shimadzu, Japan). X-ray photoelectron spectroscopy (XPS) was studied with an ESCALAB 250Xi spectrometer (Thermo Fisher Scientific, USA). The morphologies of different samples were characterized with a Supra55 field-emission scanning electron microscope (FESEM, Zeiss, Germany) equipped with energy dispersive X-ray spectrometer (EDS) and a JEM 2100 transmission electron microscope (TEM, JEOL, Japan), respectively. The N_2 adsorption/desorption isotherms were measured by using an ASAP 2010 specific surface area and pore size analyzer (Micromeritics, USA). X-ray diffraction (XRD) patterns were recorded on a Rigaku D/max 2500PC diffractometer. Thermogravimetry analysis (TGA) was performed on a TGA 209 F3 thermal analyzer (Netzsch, Germany) in N_2 atmosphere. The electrochemical experiments including cyclic voltammetry (CV), electrochemical impedance spectroscopy (EIS) and galvanostatic charge/discharge (GCD) testing were carried out using a CHI 660D electrochemical workstation (China).

Preparation of graphene oxide (GO). GO was prepared according to the method reported by Marcano et al.¹ A mixture of concentrated H_2SO_4 and H_3PO_4 (120:13.3 mL) was added to the mixture of graphite flakes and KMnO_4 (1.0:6.0 g), producing a slight exotherm to ~ 35 °C. The mixture was heated to 50 °C and stirred for 12 h, and then it was cooled to room temperature and poured onto ice (~ 135 mL) with 30% H_2O_2 (1 mL). The filtrate was centrifuged, and the supernatant was decanted away. The remaining solid material (GO) was washed thoroughly in succession with 1 M HCl and water, and finally it was dried at room temperature.

Preparation of PANI-grafted reduced graphene oxide aerogels (RGOA-PANI). 100 mg of GO was dispersed in 10 mL of water by ultrasonication, and then 100 mg of p-aminobenzoic acid and 4 mL of concentrated hydrochloric acid were added into the GO suspension and kept in an ice bath. Next, 3 mL of NaNO₂ aqueous solution (0.25 M) was added into the above suspension under stirring for 30 min. Subsequently, the resultant suspension was continuously stirred for another 6 h at an elevated temperature of 60 °C, and the obtained mixture was centrifuged. The precipitates were washed thoroughly in succession with methyl alcohol and water, dried overnight at 65 °C, and diazotized graphene oxide (d-GO) was obtained.

150 mg of the d-GO was dispersed in 60 mL of ethylene glycol by ultrasonication, and then 1.5 mL of ammonia water was added into the suspension of d-GO. Next, the resultant dark brown solution was transferred to a Teflon lined autoclave (100 mL) for solvothermal reaction at 180 °C. After 10 h, the precipitates were filtered, washed thoroughly with water, freeze-dried in a vacuum lyophilizer at -42 °C for 24 h, and amidated and reduced d-GO aerogels (RGOA) were obtained.

100 mg of the obtained RGOA was dispersed in 100 mL of 1 M HCl and stirred for 1 h, and then 0.2 mL of aniline (distilled under reduced pressure before use) was added into the RGOA suspension kept in an ice bath and stirred for 30 min. 120 mg of ammonium persulfate (APS) was dissolved in 1 M HCl (100 mL), and then the APS solution was added dropwise to the above suspension. The reaction was allowed for 9 h with continuous stirring, and the resultant products were filtered, washed with water, and freeze-dried at -42 °C for 24 h to obtain PANI-grafted RGOA, which was denoted as RGOA-PANI.

For control experiments, reduced graphene oxide aerogels were prepared by direct amidation of GO followed by freeze-drying (without diazotization of GO) and denoted as RGOA-1. Covalent functionalization of the RGOA-1 with PANI was also carried out under the same conditions as RGOA, and the resultant PANI-grafted RGOA-1 was denoted as RGOA-1-PANI. Also in this work, pure PANI was prepared by the same procedures without the addition of RGOA or RGOA-1 during the chemical oxidative polymerization of aniline.

Electrochemical measurements. All electrochemical experiments were carried out in a conventional three-electrode cell consisting of a glassy carbon electrode (GCE, 3 mm in diameter) modified with different active materials as the working electrode, a platinum foil as the auxiliary electrode and a KCl saturated calomel electrode (SCE) as the reference electrode. 1 M H₂SO₄ was used as the electrolyte. The working electrode was fabricated by dropping 10 μ L of the dispersion of different active materials (2 mg mL⁻¹) onto the surface of the GCE and allowed to dry in ambient air (areal mass loading: 0.283 mg cm⁻²). Cyclic stability of different active materials was studied by repeating the GCD testing at a current density of 10 A g⁻¹. EIS was carried out in the frequency range from 10⁶ to 0.01 Hz with an alternating sinusoidal signal of 5 mV, and the equivalent circuit was simulated by the ZSimpWin software. The specific capacitance (C_s) can be calculated from the GCD curves according to the following equation²:

$$C_s = \frac{I \times t}{m \times V} \quad (1)$$

where C_s is the specific capacitance (F g⁻¹), I is the charging-discharging current (A), t is the discharging time (s), m is the mass of the active materials modified on the surface of GCE (g), and V represents the voltage change during the discharging process (V).

FT-IR spectra of GO, d-GO and RGOA

Successful diazotization of GO and amidation/reduction of d-GO during the preparation of RGOA can be verified by the FT-IR spectra of GO, d-GO and RGOA (Fig. S1). For GO and d-GO, the broad peak centered at ~ 3425 cm⁻¹ is attributed to the stretching vibrations of O-H, and the two peaks at 1728 and 1415 cm⁻¹ correspond to C=O stretching and C-O stretching, respectively.^{3,4} The small peak at 1629 cm⁻¹ is due to the aromatic C=C.³ Noted that compared with GO, there are two additional peaks on d-GO at 1118 and 790 cm⁻¹, which can be assigned to the aromatic C-H in-plane bending (1118 cm⁻¹) and C-H out of plane for the 1,4-substituted aromatic ring stretching (790 cm⁻¹), respectively.⁵ The slight differences between GO and d-GO indicate that covalent attachment of aryl groups to GO is achieved via diazotization and GO is successfully converted to d-GO. Amidation/reduction of the d-GO was carried out by using ethylene glycol and ammonia water as solvent and nitrogen precursor respectively, and the

peak intensities of the oxygen-containing groups are greatly decreased on the resultant RGOA; meanwhile, several new bands appear on the spectra of RGOA at 3300–3600 cm^{-1} (N–H stretching of the amine groups), 1560 cm^{-1} (N–H bending vibration) and 1020 cm^{-1} (C–N stretching), respectively.^{6,7} The intensity decrease of the oxygen-containing groups and the emergence of the N-related bands on the spectra of RGOA are indicative of successful amidation and reduction of d-GO.

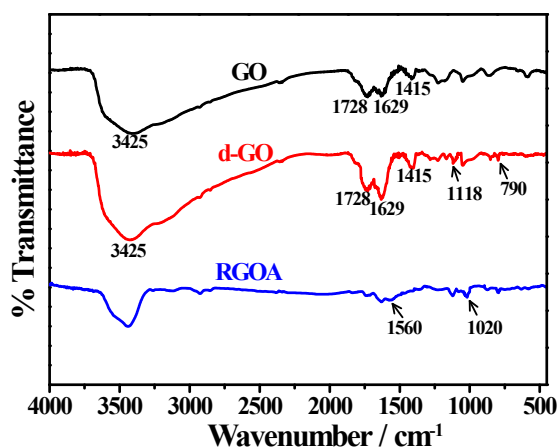


Figure S1. FT-IR spectra of GO, d-GO and RGOA.

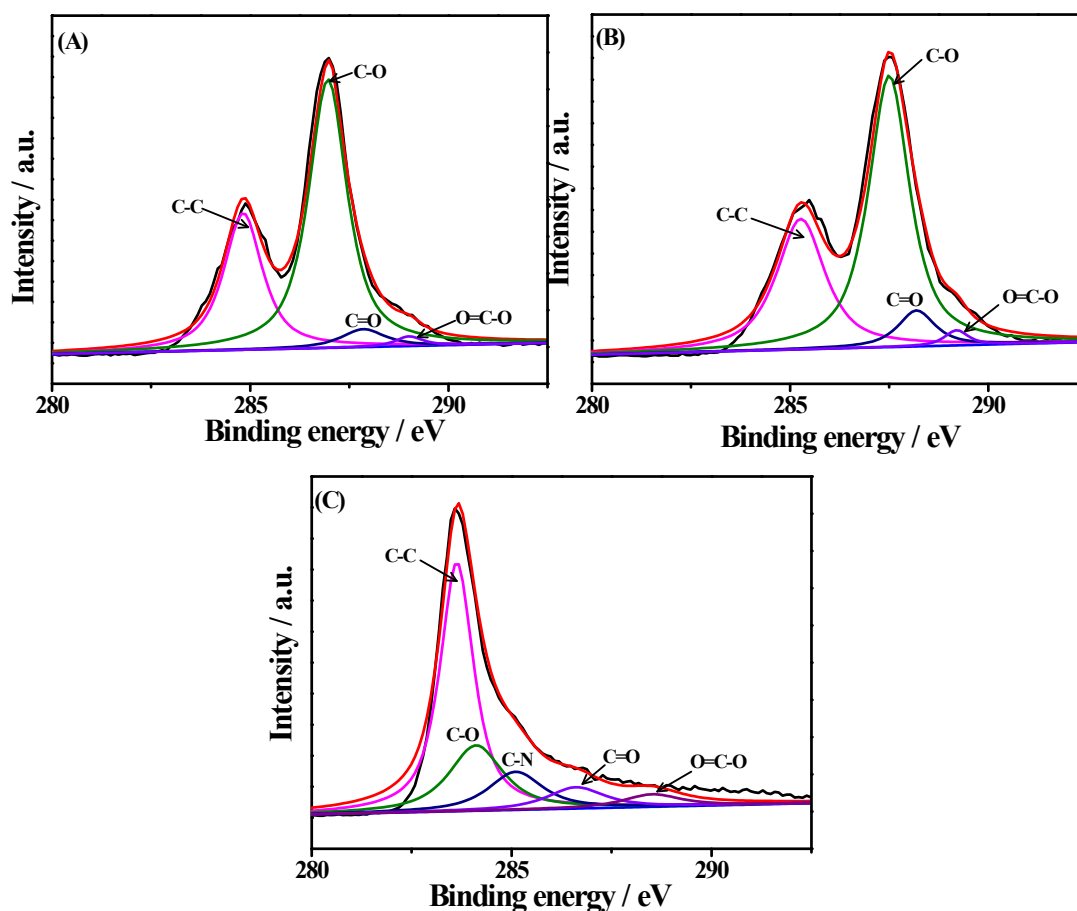


Figure S2. Carbon 1s XPS profile of GO (A), d-GO (B) and RGOA-1 (C).

C 1s XPS of GO, d-GO and RGOA-1

XPS was employed to analyze GO, d-GO and RGOA-1. The C 1s XPS of GO (Fig. S2A) and d-GO (Fig. S2B) clearly indicate the presence of four components corresponding to carbon atoms in different functional groups: non-oxygenated ring C (284.5 eV), C in C–O bonds (286.9 eV), carbonyl C (C=O, 288.0 eV) and carboxylate C (O–C=O, 289.0 eV).^{8,9} The C/O atomic ratio in d-GO (1.71) is a little higher than that in GO (1.47), which might be attributed to the covalent attachment of aryl groups to GO by diazotization. On the other hand, the peak intensities of C=O and O–C=O components in d-GO are higher than those in GO, further indicating successful diazotization of GO and introduction of aryl groups to the resultant d-GO. Fig. S2C is the C 1s XPS of RGOA-1. A new component of C–N (285.9 eV)¹⁰ is observed, which is most likely due to the introduction of amino groups to the RGOA-1 by direct amidation/reduction of GO.

SEM and TEM images of RGOA-1, RGOA, PANI and RGOA-1-PANI

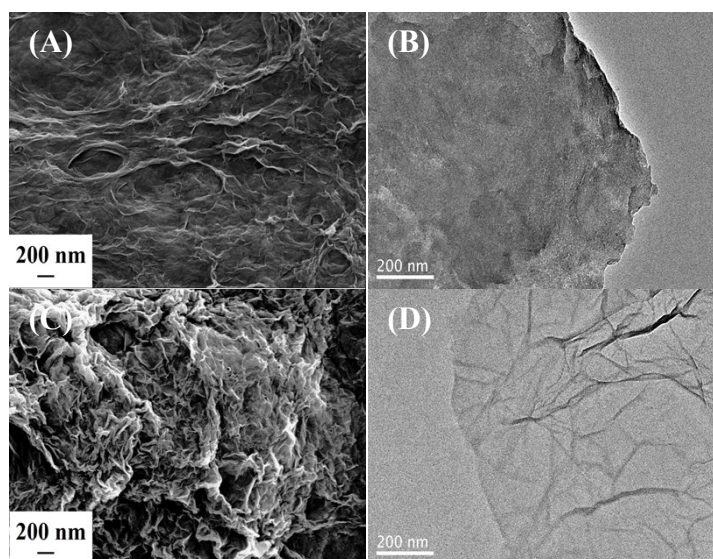


Figure S3. SEM (A, C) and TEM (B, D) images of RGOA-1 (A, B) and RGOA (C, D).

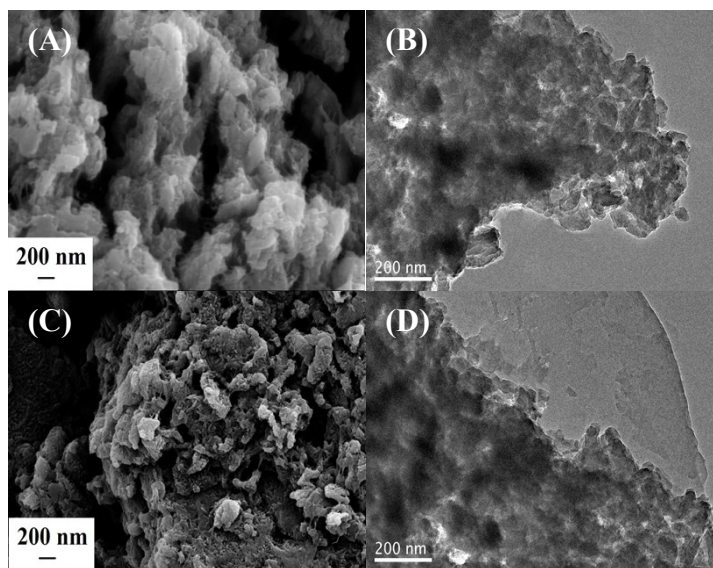


Figure S4. SEM (A, C) and TEM (B, D) images of PANI (A, B) and RGOA-1-PANI (C, D).

EDS analysis of RGOA and RGOA-PANI

The EDS analysis of RGOA and RGOA-PANI are shown in Fig. S5, and the results reveal that both the samples are mainly composed of C, O and N. The atomic percentages of RGOA-PANI are analyzed to be 79.1% (C), 4.9% (O) and 15.9% (N), and RGOA are analyzed to be 75.9% (C), 14.2% (O) and 9.8% (N). Compared with RGOA, the higher atomic percentage of N in RGOA-PANI implies that PANI is successfully grafted to RGOA.

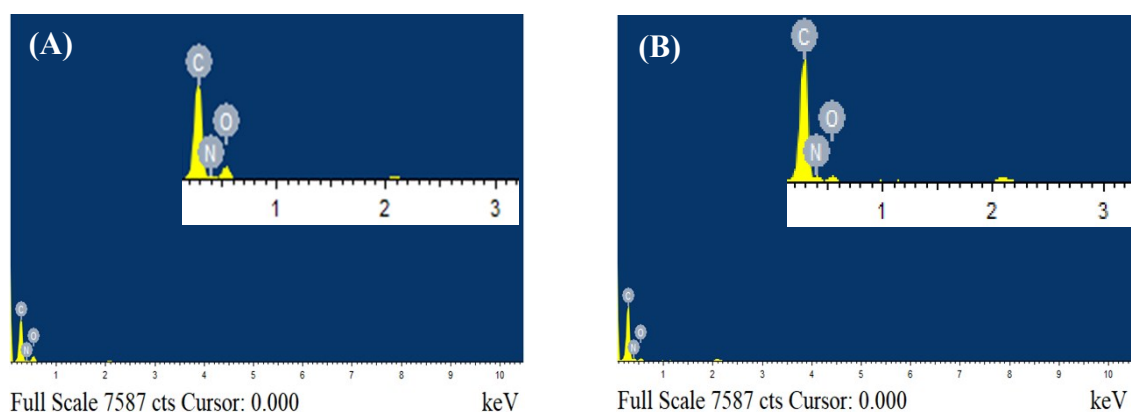


Figure S5. EDS analysis of RGOA (A) and RGOA-PANI (B).

N₂ adsorption/desorption isotherms and pore-size distributions of RGOA-PANI

The N₂ adsorption/desorption isotherms and corresponding pore size distributions of RGOA-PANI are shown in Fig. S5. RGOA-PANI exhibits a type IV isotherm with an obvious hysteresis loop (Fig. S5A), indicating the presence of mesopores.¹¹ The total pore volume and mean pore diameter of RGOA-PANI are about 0.0027 cm³ g⁻¹ and 2.836 nm (Fig. S5B), the mesoporous structure of RGOA-PANI is more beneficial for enhancing capacitance by providing a channel for fast ion transport and a low resistance for charge transfer, and these features of RGOA-PANI make it a promising candidate to shorten the diffusion pathway of electrolytes, leading to good capacitive behavior.²

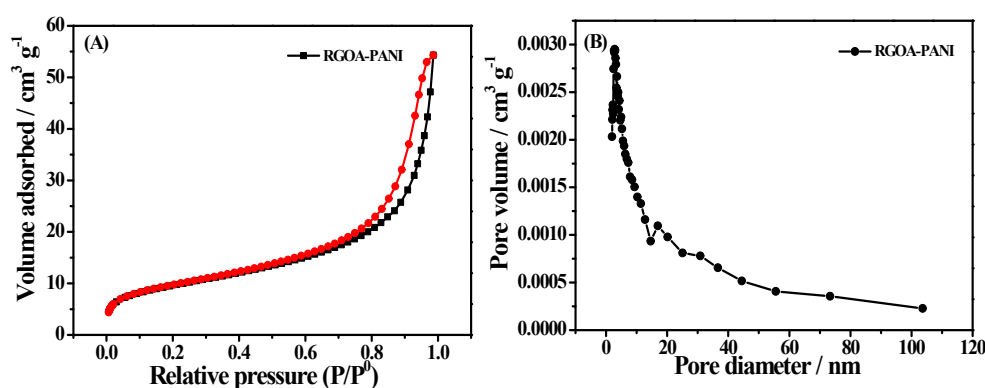


Figure S6. N₂ adsorption/desorption isotherms (A) and pore-size distributions (B) of RGOA-PANI. Temperature, 77 K.

TGA analysis of RGOA, RGOA-1, PANI, RGOA-PANI and RGOA-1-PANI

The TGA results of different samples including RGOA, RGOA-1, PANI, RGOA-PANI and RGOA-1-PANI are shown in Fig. S6. As can be seen, all these samples show a little mass loss below 120 °C due to the deintercalation of H₂O.¹² The pyrolysis of labile oxygen-containing functional groups and acidic residues (such as -OH, -CO, and -COO) in RGOA, RGOA-1 leads to a major mass loss commencing at about 200 °C. At 800 °C, the mass loss of RGOA (48%) is a little higher than that of RGOA-1 (43%), which is most likely due to the decomposition of the aryl groups introduced to RGOA. As previously reported, PANI starts to decompose at a relatively low temperature less than 150 °C and is completely oxidized at about 660 °C,¹³ and the residues of carbonized fragments are remained even at 800 °C. The mass losses of PANI, RGOA-1-PANI and RGOA-PANI from 130 to 660 °C are 45.3%, 30.6% and

29.9%, respectively, and the mass losses of the three materials are mainly attributed to the decomposition of PANI. At around 260 °C PANI and RGOA-1-PANI have a rapid mass loss, whereas the mass loss of RGOA-PANI is relatively slow at this temperature. The higher thermal stability of RGOA-PANI might be ascribed to the stronger interactions between PANI and RGOA via covalent connection.

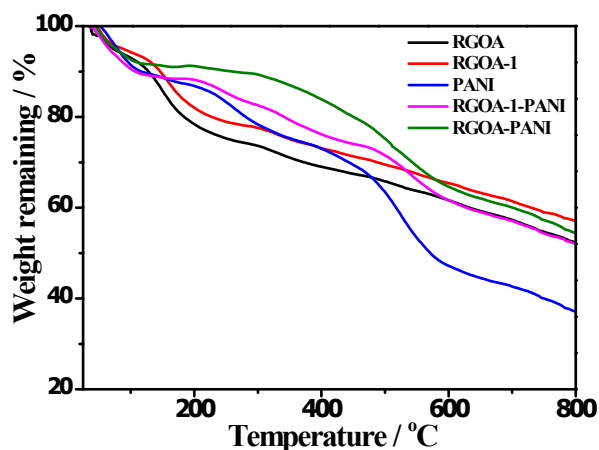


Figure S7. TGA analysis RGOA, RGOA-1, PANI, RGOA-PANI and RGOA-1-PANI in N₂ atmosphere at a heating rate of 10 °C min⁻¹.

XRD patterns of GO, d-GO, RGOA-1, RGOA, PANI and RGOA-PANI

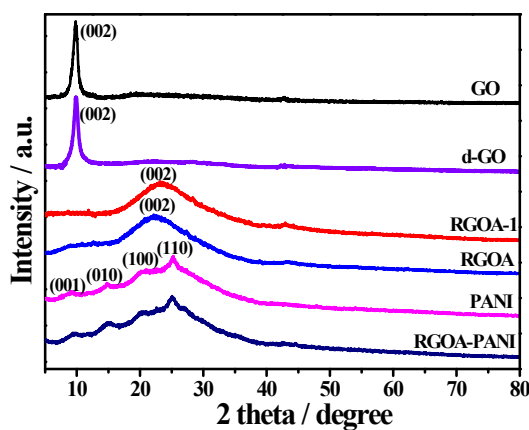


Figure S8. XRD patterns of GO, d-GO, RGOA-1, RGOA, PANI and RGOA-PANI.

Electrochemical performances of RGOA-PANI and other active materials

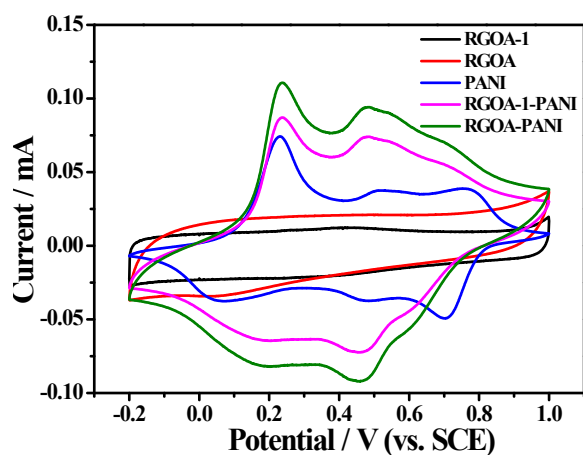


Figure S9. Cyclic voltammograms of RGOA, RGOA-1, PANI, RGOA-PANI and RGOA-1-PANI in 1 M H_2SO_4 at a scan rate of 5 mV s^{-1} .

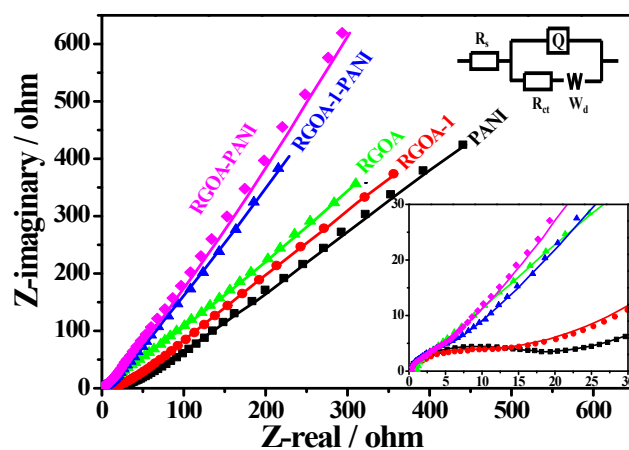


Figure S10. Nyquist plots of RGOA-PANI, RGOA-1-PANI, RGOA, RGOA-1 and PANI. Inset: corresponding equivalent circuit (top), where R_s represents the ohmic resistance of electrolyte and the internal resistance of electrode, R_{ct} represents the interfacial charge transfer resistance, W_d represents the Warburg resistance, and Q represents the constant phase element; enlargement of the Nyquist plots in the high frequency region (bottom).

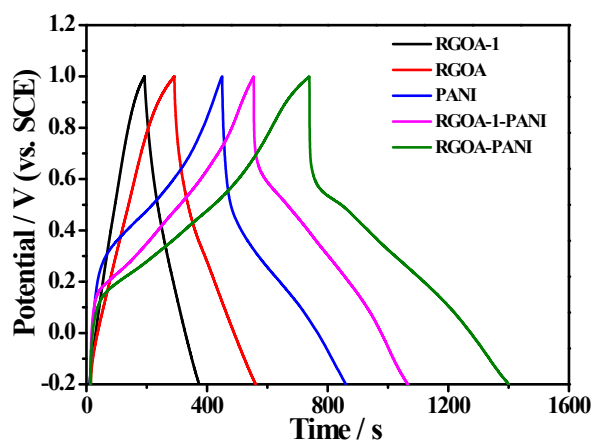


Figure S11. GCD curves of RGOA, RGOA-1, PANI, RGOA-PANI and RGOA-1-PANI in 1 M H₂SO₄ at a current density of 1 A g⁻¹.

Table S1. Comparison of capacitance between RGOA-PANI and other active materials at 1 A g⁻¹.

Samples	Capacitance	Mass loading	References
graphene/PANI	448 F g ⁻¹	0.36 mg cm ⁻²	14
RGO/PANI	410 F g ⁻¹	1.5 mg cm ⁻²	15
RGO/PANI	483 F g ⁻¹	1.6 mg cm ⁻²	16
graphene/PANI	497.9 F g ⁻¹	1~1.33 mg cm ⁻²	17
RGOA-PANI	553 F g ⁻¹	0.283 mg cm ⁻²	This work

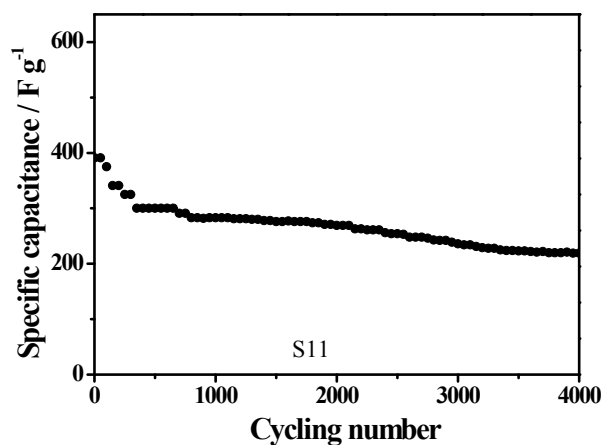


Figure S12. Longer cycling performance test of RGOA-PANI at a current density of 10 A g⁻¹.

References

- 1 D. C. Marcano, D. V. Kosynkin, J. M. Berlin, A. Sinitskii, Z. Sun, A. Slesarev, L. B. Alemany, W. Lu and J. M. Tour, *ACS Nano*, 2010, **4**, 4806.
- 2 B. H. Wang, Y. Qin, W. S. Tan, Y. X. Tao and Y. Kong, *Electrochim. Acta*, 2017, **241**, 1.
- 3 X. M. Feng, R. M. Li, Y. W. Ma, R. F. Chen, N. E. Shi, Q. L. Fan and W. Huang, *Adv. Funct. Mater.*, 2011, **21**, 2989.
- 4 Z. H. Liu, H. H. Zhou, Z. Y. Huang, W. Y. Wang, F. Y. Zeng and Y. F. Kuang, *J. Mater. Chem. A*, 2013, **1**, 3454.
- 5 S. P. Zhou, H. M. Zhang, Q. Zhao, X. H. Wang, J. Li and F. S. Wang, *Carbon*, 2013, **52**, 440.
- 6 L. F. Lai, L. W. Chen, D. Zhan, L. Sun, J. P. Liu, S. H. Lim, C. K. Poh and Z. X. Shen, J. Y. Lin, *Carbon*, 2011, **49**, 3250.
- 7 W. F. Zhang, S. S. Wang, J. Y. Ji, Y. Li, G. L. Zhang, F. B. Zhang and X. B. Fan, *Nanoscale*, 2013, **5**, 6030.
- 8 S. Stankovich, R. D. Piner, X. Q. Chen, N. Q. Wu, S. B. T. Nguyen and R. S. Ruoff, *J. Mater. Chem.*, 2006, **16**, 155.
- 9 Y. S. Ye, Y. N. Chen, J. S. Wang, J. Rick, Y. J. Huang, F. C. Chang and B. J. Hwang, *Chem. Mater.*, 2012, **24**, 2987.
- 10 S. Stankovich, D. A. Dikin, R. D. Piner, K. A. Kohlhaas, A. Kleinhammes, Y. Jia, Y. Wu, S. B. T. Nguyen and R. S. Ruoff, *Carbon*, 2007, **45**, 1558.
- 11 K. Xia, Q. Gao, J. Jiang and J. Hu, *Carbon*, 2008, **46**, 1718.
- 12 X. Wang, T. Wang, C. Yang, H. Li and P. Liu, *Appl. Surf. Sci.*, 2013, **287**, 242.

- 13 N. A. Kumar, H. J. Choi, Y. R. Shin, D. W. Chang, L. Dai and J. B. Baek, *ACS Nano*, 2012, **6**, 1715.
- 14 M. Hassan, K. R. Reddy, E. Haque, S. N. Faisal, S. Ghasemi, A. I. Minett and V. G. Gomes, *Compos. Sci. Technol.*, 2014, **98**, 1.
- 15 H. Qiu, X. Han, F. Qiu and J. Yang, *Appl. Surf. Sci.*, 2016, **376**, 261.
- 16 W. Dai, L. Ma, M. Gan, S. Wang, X. Sun, H. Wang, H. Wang and T. Zhou, *Mater. Res. Bull.*, 2016, **76**, 344.
- 17 R. Wang, M. Han, Q. Zhao, Z. Ren, X. Guo, C. Xu, N. Hu and L. Lu, *Sci. Rep.*, 2017, **7**, DOI: 10.1038/srep4456.